Chalcogenide Letters Vol. 15, No. 12, December 2018, p. 605 - 613

FORMATION AND NEGATIVE CAPACITANCE EFFECT IN $Au/Bi_2O_3/ZnS/Ag$ HETEROJUNCTIONS DESIGNED AS MICROWAVE RESONATORS

S. E. AL GARNI[a,b], A. F. QASRAWI[c,d,*]

[a]*Physics Department, Faculty of Science- Al Faisaliah, King Abdulaziz University, Jeddah- Saudi Arabia*

[b]*Department of Physics, Faculty of Science, University of Jeddah, Jeddah, Saudi Arabia*

[c]*Department of Physics, Arab American University, Jenin, Palestine*

[d]*Group of physics, Faculty of Engineering, Atilim University, 06836 Ankara, Turkey*

In this article, the physical design, energy band diagram, temperature dependent electrical resistivity and the impedance spectroscopy measurements of the $Au/Bi_2O_3/ZnS/Ag$ isotype heterojunction devices are reported. The devices are prepared by the thermal evaporation technique under vacuum pressure of 10^{-5} mbar. Structural, compositional and morphological studies has shown the presence of an expansion in the lattice of Bi_2O_3 associated with increased strain and dislocation density and decreased grain size as a result of ZnS interfacing. The design of the band diagram indicated that the formed heterojunction exhibit large valence and conduction band offsets that forces charge accumulation at the interface. The $Au/Bi_2O_3/ZnS/Ag$ device displays negative capacitance (NC) effect in the frequency domain of 0.01-1.50 GHz. The NC effect is interrupted by a resonance-antiresonance phenomenon in the frequency domain of 0.90-1.07 GHz. In addition to the NC effects, the device under study exhibited reflection coefficient and return loss spectra that nominate it for use as microwave cavities or as low pass band filters.

(Received October 23, 2018; Accepted December 5, 2018)

Keywords: Bi_2O_3/ZnS, X-ray diffraction, Band filters, Band diagram, Microwave cavity

1. Introduction

Heterojunction devices comprising bismuth oxide are of interest owing to their technological applications. In one of the recent photocatalytic experiments it was observed that the Bi_2O_3/Bi_2WO_6 composite can reveal a higher photocatalytic activity for RhB degradation under visible-light irradiation than that of pure Bi_2O_3 and Bi_2WO_6 [1]. In another work [2], Bi_2O_3/Si interfaces are reported to exhibit appropriate features for photovoltaic applications. Bi_2O_3/Si heterojunction device of thickness of 600 nm displayed open circuit voltage of 0.24 V associated with short circuit current and efficiency of values of 41 mA/cm^2 and 4.08%, respectively [2]. In addition, Bi_2O_3 films which are deposited onto cellulose fiber paper exhibited nonlinear electrical response that nominates it for production of supercapacitors and thin film transistors [3]. The flexible cellulose-bismuth oxide interface exhibited merits of threshold voltage at 1.0 V and high mobility value of 0.63 cm^2/Vs. These heterojunction devices show negative resistance effect which make it suitable for use as resonant tunneling diodes.

One of the $B_{i2}O_3$ based heterojunctions is the Bi_2O_3/ZnS interfaces. This interface which is prepared by the phase-inversion method [4] is reported to be suitable for degradation of Rhodamine B from water. It exhibits smart features as photocatalytic material. Recalling that in our previous investigations [5] we have shown that the $In/Bi_2O_3/Au$ and $Yb/Bi_2O_3/Au$ interfaces can perform as microwave traps, we, here in this work, are motivated to explore the fundamental properties and features of the Bi_2O_3/ZnS system to widen its range of applications. Particularly, the

* Corresponding author: atef.qasrawi@aaup.edu

crystalline nature, morphology, composition and impedance spectroscopy studies on the Au/Bi_2O_3/ZnS heterojunctions will be carried out to state the possible electronic applications of these thin film devices.

2. Experimental details

The electronic device is prepared in a vacuum evaporation system using the thermal evaporation technique under a pressure of 10^{-5} mbar. The fabrication of the device includes a pure (99.98%) Au film coated onto ultrasonically cleaned glass substrates and a 200 nm thick bismuth oxide layers coated onto the Au substrate. As the geometrical design which is shown in inset-1 of Fig. 1 shows, the Au/Bi_2O_3 films are partially coated with ZnS film of thickness of 500 nm. Both parts of the device are contacted with circularly shaped Ag point contacts of area of $7.3\times 10^{-3}\ cm^2$. The samples are studied by energy dispersive X-ray diffraction unit attached to a scanning electron microscope and by X-ray diffraction unit using Miniflex 600 XRD unit. The impedance spectroscopy is measured in the frequency domain of 10–1500 MHz at room temperature using Agilent 4291B 1.0M–1.8 GHz impedance analyzer. The connections to the fixture (16453A dielectric material test fixture,) were made by AP-7 connector attached to the analyzer.

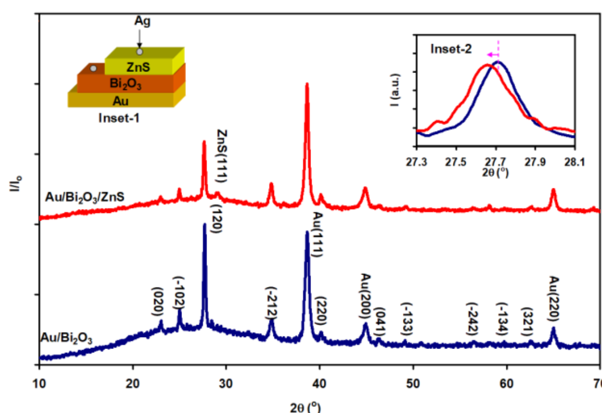

Fig. 1. The X-ray diffraction patterns for the Au/Bi_2O_3 and Au/Bi_2O_3/ZnS films. Inset-1 show the geometrical design and inset-2 show the shift in the maximum peak due to the coating of ZnS onto Au/Bi_2O_3.

3. Results and discussion

The results of the X-ray diffraction technique which is carried out on the device are shown in Fig. 1. In accordance with the displayed patterns both of the Au/Bi_2O_3 and Au/Bi_2O_3/ZnS are of polycrystalline nature. Two intensive peaks are observed in the XRD of Au/Bi_2O_3. The indexing of these peaks as well as all other peaks in accordance with the “TREOR 92” software packages reveal a face centered cubic crystal structure for the Au films and monoclinic structural phase for the Bi_2O_3 thin films. The calculated unit cells parameters that allowed the indexing which is illustrated in the figure are 4.029 Å for Au film and values of a=5.8486, b=8.1661, c=7.5097 Å and $\beta = 113^o$ for the Bi_2O_3 films. The data is consistent with the crystallography open database (COD) cards; COD-1100138 and COD-9012546 that are reported for Au and monoclinic Bi_2O_3, respectively. On the other hand, the coating of Bi_2O_3 with ZnS display the diffraction patterns which are shown in the same figure. The patterns which are collected from the surface of the Bi_2O_3/ZnS contained only one additional peak centered at $2\theta = 29.05^o$ that coincides with that reported in card COD-1101051. This peak refers to the cubic phase of ZnS and exhibit lattice parameters of value of 5.317 Å. The difference in the crystalline nature and lattice parameters

indicate deformed nature of growth due to the large lattice misalignment between Au and Bi_2O_3 and between Bi_2O_3 and ZnS. The shift in the major peak of Bi_2O_3 due to the coating with ZnS is illustrated in inset-2 of Fig. 1. As the pink colored arrow shows the maximum peak shift toward lower angles indicating the expansion of the lattice. It was reported that the expansion in the lattice usually results from the replacement of the larger ionic radius with smaller one [6]. The same rule should apply for our films as the ionic radius of Zn^{+2} (74 pm) is less than that of Bi^{+3} (104 pm) [7]. It was also mentioned that the filling of the bismuth vacancy by Zn ions in Bi_2O_3-ZnO system may cause tailoring of the nonlinear characteristics of ZnO [8].

In an attempt to gain information about the effect of ZnS on the structural parameters of Bi_2O_3, the strain ($\in$), grain size (D) and defects density (δ) in the films are determined from the major peaks broadening and 2θ values before and after coating with ZnS. The structural parameters are calculated with the help of the early published relations [9]. An increase in $\in$ and δ associated with decrease in the values of D from 3.52×10^{-3}, $2.1\times 10^{11}\ cm^{-2}$ and from 43 nm to 4.14×10^{-3}, $2.9\times 10^{11}\ cm^{-2}$ and 37 nm, respectively, is observed upon coating Au/Bi_2O_3 films with ZnS. The structural modifications that arise from the interfacing of the two materials can be explained in the light of atomic interactions and bonding mechanisms. Since the bond length of Zn-S being 2.30 Å [10] is larger than the bonds length of Zn-O (1.94 Å [11]) and because the bond length of Zn-O is shorter than that of Bi-O (2.42 Å [12]), substitution of Zn in vacant sites of Bi forms the strongest bonding mechanism. The density functional theory calculations with local density approximations using linear combination of atomic orbitals for the ZnO-ZnS system arrived at the result that the oxygen vacancy distorts the structure. While the Zn-Zn bonds forms with local lengths between Zn-Zn atoms causing bond contraction of 0.50 Å, the Zn-O bond length expands by 0.05 Å [10]. It is reported that the formation of oxygen vacancy is associated with charge transfer forcing accumulation of Zn atoms around O vacancy whereas no charge accumulation is observed at the O sites near the O vacancy. The introduction of the O vacancies is believed to be the main reason for the increase in the defect density [10].

Fig. 2 (a) display the scanning electron microscopy images which are recoded from the surface of Bi_2O_3/ZnS film. The images which are collected from the Bi_2O_3 surface are shown as inset-1 of Fig. 2 (a). For an enlargement of 60,000 times of a working distance of 8 mm, trapezoidal and rectangular shaped grains of average size of 45 nm are observed for the Bi_2O_3 films (inset-1 of Fig. 2). The same SEM image (Fig. 2) which is collected from the surface of Bi_2O_3/ZnS Display circular grains of average size of 35 nm. The value is close to that we detected from the X-ray diffraction analysis. The reduction in the grain size should be assigned to the lattice expansion [13] as we mention in the proceeding discussion. It was reported that transition from polycrystalline to amorphous phases in silicon which is dominated by reduction of grain sizes and expansion of lattice parameters is thermodynamically assigned to the increase in the free energy. The free energy arises from the reduction in the driving force which causes the crystalline-to-amorphous transitions. The lattice expansion increases the elastic energy which is in turn increases the specific surface energy of small crystallites [13]. On the other hand, Fig. (b) displays the energy dispersive X-ray analysis for the Bi_2O_3/ZnS heterojunctions. The spectra display the existence of glass, ZnS and bismuth oxide atoms as expected. Various regions on the sample surface are scanned. The maximum error in the atomic content is ~10% of the measured value . The atomic compositions of the studied samples are found to be 49.7 at.% Zn and 51.3 at.% S for the ZnS and 38.3 at. % Bi and 61.7 at. % O for Bi_2O_3. The deviation from the correct stoichiometry is still within the acceptable experimental error.

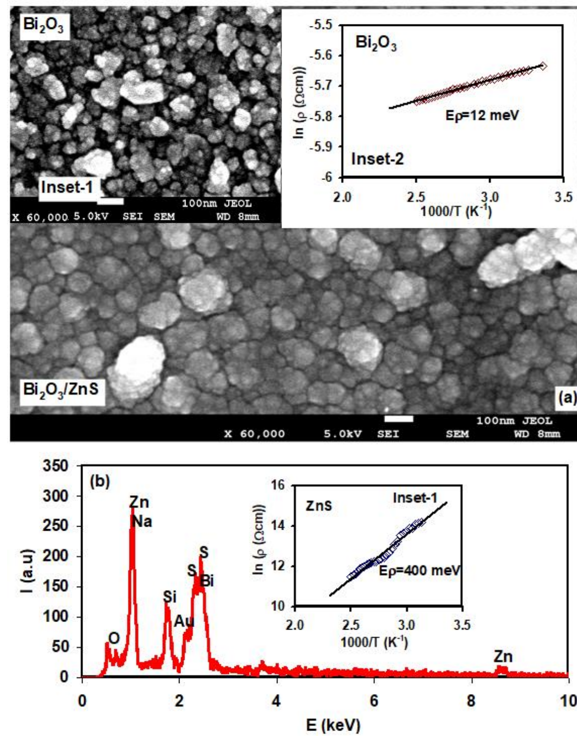

Fig. 2. (a) The scanning electron microscopy results for an enlargement of 60000 times from the surface of the Au/Bi_2O_3/ZnS/Ag device and (b) the energy dispersive X-ray spectra for Au/Bi_2O_3/ZnS/Ag device. The insets of (a) and (b) show the Arrhenius plots of the electrical resistivity of the Bi_2O_3 and ZnS, respectively.

The tests using the hot probe technique on the Bi_2O_3 and on ZnS films have shown that both samples exhibit *n*-type conductivity indicating the isotype of heterojunction. To determine the work function of these two materials, temperature dependent electrical resistivity measurements($\rho(T)$) for amples grown onto glass substrates are carried out in the temperature range of 300-400 K. The $\rho(T)$ variations which are shown in inset-2 of Fig. 2 (a) and inset-1 of Fig. 2 (b)), for Bi_2O_3 and ZnS films, respectively, have shown that while ZnS exhibits resistivity activation energy (E_ρ) of 400 meV, the slope of the Arrhenius plot of the resistivity of Bi_2O_3 revealed E_ρ value of 11 meV. The impurity level in ZnS is deep causing a Fermi level (E_F) at ~200 meV. The Fermi level in Bi_2O_3 is at ~5.5 meV below the conduction band. The monoclinic Bi_2O_3 sample is, approximately, of degenerate type and satisfied the case where the Fermi level reaches the edge of the conduction band. Such information are important as they allow investigating the energy band diagram of the Bi_2O_3/ZnS system. The schematic of the energy band diagram for the isotype heterojunction is shown in Fig. 3. In accordance with the resistivity activation energies, the work function of Bi_2O_3 ($q\phi_1 = q\chi_1 + |E_{F1} - E_{c1}|$) and of ZnS ($q\phi_2 = q\chi_2 + |E_{F2} - E_{c2}|$) are 4.99 eV and 4.10 eV, respectively. Because the work function of Au (5.34 eV) is larger than that of Bi_2O_3, the Au/Bi_2O_3 interface forms a Schottky barrier. Oppositely, as the work function of Ag (4.23 eV) is sufficiently close to the work function of ZnS, the ZnS/Ag interface can be regarded as ohmic contact. In addition, since the electron affinities and energy band gaps of Bi_2O_3 and ZnS are $q\chi_1 = 4.94\ eV$ and 2.80 eV [5] and $q\chi_2$ =3.90 eV and 3.40 eV, respectively, then, the respective conduction ($\Delta E_c = q\chi_2 - q\chi_1$) and valence band ($\Delta E_v = \Delta E_g - \Delta E_g$) offsets are 1.04 and 0.41 eV. Large values of band offset are reported to play vital role in the performance of electronic devices as they disturb the carrier transport of generated carriers forcing them to accumulate at the heterointerface [14]. The formed n-n electron depletions region and electron accumulation region causes the creation of interface capacitance [15]. In addition, as the Bi_2O_3 films are approximately, degenerate exhibiting high free conduction electron concentration it may lead to the establishment of conduction channels at the interface between the ZnS and Bi_2O_3

layers. It is mentioned that at the CdO/ZnO interface, the higher carrier concentration of CdO causes a significant diffusion of charge carriers in the conduction band of ZnO near the interface forming a conducting channel at the interface in the ZnO sides [15]. It is also stated that the accumulation of electrons in ZnO films fill the trap states and as a result it improves the carrier mobility by decreasing the amount of traps states that facilitate the carrier transport [15]. Moreover, it is believed that charge accumulation at the interface of heterojunctions can be employed to produce negative capacitance [16]. This character of heterojunction devices is used for power amplification in thin film transistors and for noise reduction in microwave cavities [17].

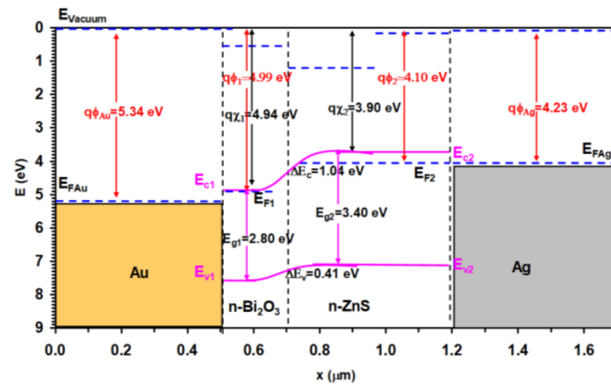

Fig. 3. The energy band diagram for the Au/Bi$_2$O$_3$/ZnS/Ag device.

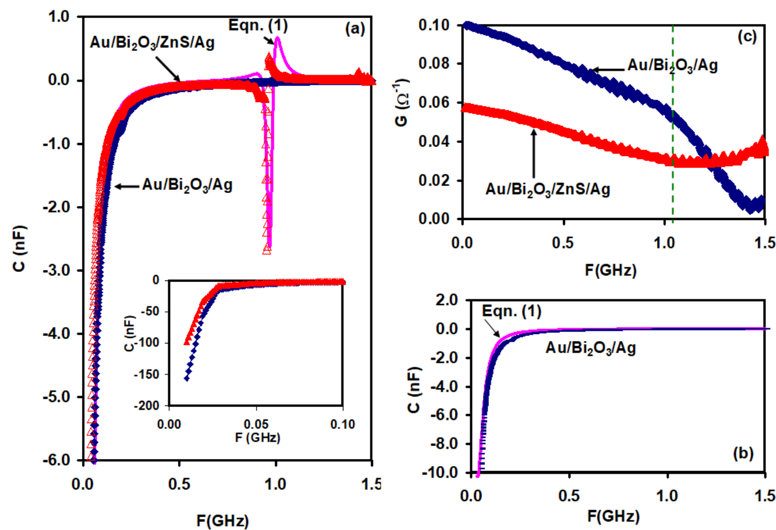

Fig. 4. (a) the capacitance spectra for the Au/Bi$_2$O$_3$/Ag and Au/Bi$_2$O$_3$/ZnS/Ag channels, (b) the capacitance spectra for Au/Bi$_2$O$_3$/Ag channel showing the agreement with the fitting of Eqn. (1) and (c) the conductance spectra for Au/Bi$_2$O$_3$/Ag and Au/Bi$_2$O$_3$/ZnS/Ag channels. The inset of (a) show the enlargement of the capacitance in the low frequency domain.

Fig. 4 (a) –(c) illustrates the measured capacitance (C) and conductance (G) spectra for the Au/Bi$_2$O$_3$/Ag (channel 1) and Au/Bi$_2$O$_3$/ZnS/Ag (channel 2) channels which are geometrically demonstrated in inset-1 of Fig. 1. As Fig. 4 (a) and its inset shows, a large range of negative capacitance effect is observed in both channels. The capacitance increases from -155 nF to ~ -10 pF in the frequency domain of 0.01-0.83 GHz, reflecting wide range of tunability of the devices. However, while the first channel exhibits negative capacitance effect in all the studied range of frequency (0.01-1.50 GHz), the second channel display a resonance-antiresonance phenomenon in

the frequency domain of 0.90-1.07 GHz. This additional feature of the device raised from the coating of ZnS on the surface of Bi_2O_3. To give significance to the observed negative capacitance and resonance-antiresonance phenomena, the capacitance spectra is modeled in accordance with the modified Ershov equation for negative capacitance spectra [18] which takes the form,

$$C(w) = C_o + \frac{a_1\tau_{n1}}{1+(w-w_{n1})^2\tau_{n1}^2} - \frac{a_2\tau_{n2}}{1+(w-w_{n2})^2\tau_{n2}^2} \quad (1)$$

Here, w, w_{n1}, w_{n2} are the radial frequency of signal, cutoff frequency of majority carriers in Bi_2O_3 and cutoff frequency of majority carriers in ZnS, respectively. τ_{n1} and τ_{n2} are the scattering times of charge carriers in the respective layers. $a_1$and a_2 are constant parameters and C_o is the geometrical capacitance. In this model the transient response of the capacitance spectra is assumed to be composed of negative and positive exponential components that arise from charge transport from both sides of the device. In accordance with the above equation, the capacitance values being positive or negative depends on the material and the limiting frequency which is characteristic of the material. The fitting to the experimental data which is shown by black solids lines in Fig. 4 (a) and (b) are listed in Table 1.

Table1. Fitting parameters for the capacitance spectra for the Bi_2O_3/ZnS heterojunction device.

Parameter	Au/Bi_2O_3/Ag	Au/Bi_2O_3/ZnS/Ag
$C_o(pF)$	1.0	1.0 + $C_{Ch.1}$
a_{n1}	-	1.0
a_{n2}	2.2	1.0
τ_{n1}(ns)	-	4.7
τ_{n2}(ns)	4.7	7.1
w_{n1}(GHz)	-	6.14
w_{n2}(GHz)	0.20	6.10

*$C_{ch.1}$: The capacitance obtained by Eqn.1 for channel 1

In accordance with the table, the scattering time which represents the inverse of the damping coefficient ($\gamma = \tau^{-1}$) increases from 4.7 ns to 7.1 ns upon coating of Bi_2O_3 with ZnS. The decreased damping force or electronic frictional force may be assigned to the structural modifications that are associated with isotype interfacing and the large band offsets between the Bi_2O_3 and ZnS layers. In addition, the cutoff frequency of the Bi_2O_3 channel abruptly increases from 0.20 to 6.10 GHz when wave propagate through second channels. The reason beyond this increase could be strong bonding between the Zn and O atoms as we mentioned in this article.

While the negative capacitance is mainly assigned to non-equilibrium interfacial states [18], in accordance with the above analysis, the resonance-antiresonance phenomena which are observed in Au/Bi_2O_3/ZnS/Ag channel should be assigned to the dielectric constant (degree of polarization) dynamics as it represents the degree of polarization. The oscillation of electric dipoles in response to the incident ac signal is a time dependent process. Particularly, when the frequency of the oscillating dipoles is larger than that of the propagating signal, the dipoles have the sufficient time to orient with the signal. However, when both electric dipoles whose frequency values are w_{n1}, w_{n2} and alternating current oscillate at the same frequency ($w = w_{n1}, w_{n2}$), a maximum dielectric constant value is expected due to the ability of all dipoles to oscillate with the field. The effect is associated with no free charge. Similarly as the signal frequency exceeds that of dipole, the dipole start not feeling the signal. Since the heterojunction is composed of two layers, and as each layer has its own cutoff frequency (Table 1), while one layer is at resonance, the other set all its charge carriers free due to the inability of the dipole to follow the signal. This behavior results in the observed antiresonance behavior. Other studies which

explains the origin of negative capacitance assigned it to the presence of trap states at the materials surfaces [16]. Increasing the trap states is reported to enhance the negative capacitance effect. This also explains the decrease in the value of the negative capacitance in Bi_2O_3 when coated with ZnS. As the inset of Fig. 4 (a) shows, the capacitance value decrease from -155 nF at 10 MHz to -97 nF upon coating. Such behavior may be assigned to the trap states filling by Zn in vacant sites of Bi.

Fig. 4 (c) show the conductance (G) spectra for the two channels under investigation. It is clear from the figure that the coating of the ZnS onto bismuth oxide decreased the conductance values and altered the slopes of variations of the conductance spectra. Particularly, while the conductance of the Au/Bi_2O_3/Ag decreases with increasing signal frequency following two slopes of variation above and below 1.04 GHz (dashed line in Fig. 4 (c)), the conductance of Au/Bi_2O_3/ZnS/Ag decreases with increasing frequency above 1.04 GHz and then increased with increasing signals frequency. This behavior of the conductance may be ascribed to the changes in the current transport mechanism as a result of the dynamics of surface charges as we mentioned in the capacitance spectra part [16, 18]. On the other hand, in accordance with the band diagram which is presented in Fig. 3, the modulation of the Fermi level at the interface between Bi_2O_3 and ZnS require flowing of some free electrons from the conduction band of Au/Bi_2O_3 to the valence band of ZnS so that the equilibrium case is reached. The common Fermi level for the heterojunction device is actualized by the distribution of free electrons through the depletion region between the two materials. The reduction of the free carrier density make the electrons available for conduction less and as a result the conductance decreases. From structural point of view, the large lattice mismatches between the two materials make the electronic transitions harder. This leads to less mobile carriers for electrical conduction [19].

The total effect that arises from the dynamics of capacitance and conductance spectra is screed from the impedance (Z) spectra which are displayed in Fig. 5 (a). The impedances of the first and second channels smoothly increase with increasing signal frequency below 1.15 GHz. Above this frequency value, the impedance spectra sharply increases from 19 to 79 Ω for the first channel. This sharp increase is removed when the Au/Bi_2O_3 Schottky device is coated with ZnS. The impedance spectra for the second channel exhibit maxima at 1.15 GHz and then decreases with increasing frequency in the frequency domain of 1.15-1.50 GHz. On the other hand, the magnitude of the reflection coefficients ($\rho = \frac{Z_{device}-Z_{source}}{Z_{device}+Z_{source}}$) and the return loss values ($L_r = |-20\log(\rho)|$) [20, 21] which are calculated from the impedance value are displayed in Fig. 5 (b) and (c), respectively. The ρ spectra are always less than 1.0 indicating the presence of impedance match between the source and device. This feature is important as it indicates low pass filters property. There is an attenuation in the propagating signal in all the studied frequency domain. As the return loss represents the power that is not absorbed by the channel and is therefore returned to the source, large absolute values of the L_r (i.e.: > |20| dB) imply a good match between the source and the operating channel. Both of the Fig. 5 (b) and (c) show that the ZnS coating has significantly enhanced the filtering property of the microwaves. Even though an enhancement in the filtering property is achieved by the Au/Bi_2O_3/ZnS/Ag heterojunction formation, the magnitude of the reflection coefficient and return loss values still below the standards [21] and some further issues are needed to improve the performance of the device under study.

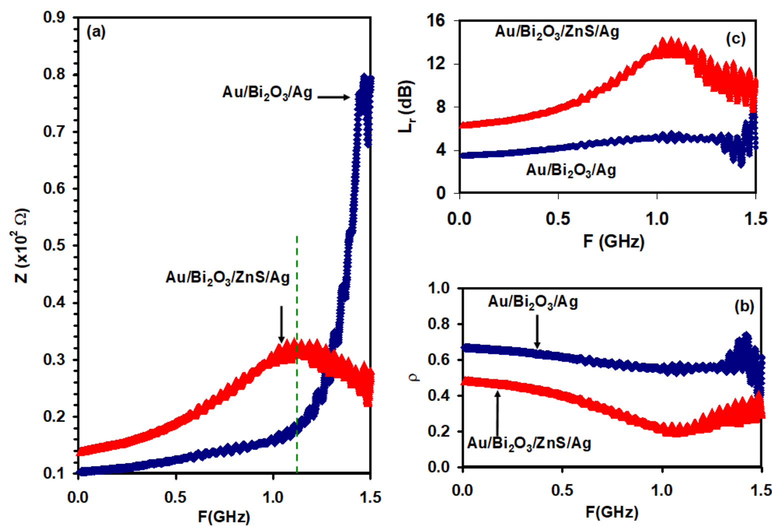

Fig. 5. (a) The impedance, (b) magnitude of reflection coefficient and (c) the return loss spectra for $Au/Bi_2O_3/Ag$ and $Au/Bi_2O_3/ZnS/Ag$ channels.

4. Conclusions

In the current study we have investigated the structural, morphological, compositional and impedance spectral analyses on Bi_2O_3 and Bi_2O_3/ZnS thin films that are grown onto Au substrates. The two channel device ($Au/Bi_2O_3/Ag$ and $Au/Bi_2O_3/ZnS/Ag$) is found to exhibit strained structure and large band offsets that allow charge accumulations and confinements. The proposed device is observed to exhibit negative capacitance (NC) effect in the $Au/Bi_2O_3/Ag$ channel. The NC effect is accompanied with resonance-antiresonance phenomena near 1.0 GHz. These properties of the device make it attractive for applications in telecommunication technologies as microwave cavities and as parasitic capacitance cancellers. Some further research is advised to improve the impedance matching properties of the Bi_2O_3/ZnS system to make it combatable with commercial cavities.

Acknowledgments

This project was funded by the Deanship of Scientific Research (DSR) at King Abdulaziz University, Jeddah, under grant No. (G:91-363-1439). The authors, therefore, acknowledge with thanks DSR for technical and financial support.

References

[1] C. Y. Yan, W. T. Yi, J. Xiong, J. Ma, IOP Conference Series: Earth and Environmental Science, IOP Publishing **128**(1), 012086 (2018).
[2]B. K. Al-Maiyaly, B. H. Hussein, A. A. Salih, A. H. Shaban, S. H. Mahdi, I. H. Khudayer, AIP Conference Proceedings, AIP Publishing, **1968**(1), 030046 (2018).
[3] Y. Wu, H. Fu, B. Li, Y. Lin, Materials Express **7**(1), 5 (2017).
[4] B. Li, J. Chu, Y. Li, M. Meng, Y. Cui, Q. Li, Y. Feng, Physica Status Solidi A, 1701061 (2018), doi.org/10.1002/pssa.201701061.
[5] N. M. Khusayfan, A. F. Qasrawi, H. K. Khanfar, Materials Science in Semiconductor Processing **64**, 63 (2017), doi.org/10.1016/j.mssp.2017.02.028.
[6] J. Janbua, S. Niemchareon, R. Muanghlua, N. Vittayakorn, Ferroelectric **490**(1), 13 (2016).
[7] F. C. Correia, P. B. Salvador, J. M. Ribeiro, A. Mendes, C. J. Tavares, Vacuum **152**, 252 (2018), doi.org/10.1016/j.vacuum.2018.03.033.

[8] A. Mekap, P. R. Das, R. N. P. Choudhary, Journal of Electronic Materials **45**(8), 4338 (2016).
[9] S.R. Alharbi, A. F. Qasrawi, Current Applied Physics **18**(8), 946 (2018).
[10] A. Ali, G. Rahman, T. Ali, M. Nadeem, S. K. Hasanain, M. Sultan, Physica E: Low-dimensional Systems and Nanostructures **103**, 329 (2018), doi.org/10.1016/j.physe.2018.06.028.
[11] X. M. Meng, X. Zhang, P. F. Qi, Z. A. Zong, F. Jin, Y. H. Fan, RSC Advances **7**(9), 4855 (2017).
[12] W. Gu, F. Teng, Z. Liu, Z. Liu, J. Yang, Y. Teng, Journal of Photochemistry and Photobiology A: Chemistry **353**, 395 (2018), doi.org/10.1016/j.jphotochem.2017.11.047.
[13] C. C. Koch, Journal of non-crystalline solids **117**, 670 (1990), doi.org/10.1016/0022-3093(90)90620-2
[14] K. Kodama, R. Takabe, T. Deng, K. Toko, and T. Suemasu, Japanese Journal of Applied Physics **57**(5), 050310 (2018).
[15] A. Bera, R. Thapa, K. K. Chattopadhyay, B. Saha, Journal of Alloys and Compounds **632**, 343 (2015). doi.org/10.1016/j.jallcom.2015.01.168
[16] Q. Niu, N. I. Crăciun, G. J. A. Wetzelaer, P. W. Blom, Physical review letters **120**(11), 16602 (2018).
[17] S. Salahuddin, S. Datta, Nano letters **8**(2), 405 (2008).
[18] N. M. Khusayfan, A. F. Qasrawi, H. K. Khanfar, Materials Research Express **5**(2), 026303 (2018).
[19] S. M. Sze, K. K. Ng. Physics of semiconductor devices, John wiley & sons, 2006.
[20] D. M. Pozar, Tramsmission Lines and Waveguides, 143 (2005).
[21] S. E. Al Garni, A. F. Qasrawi, Chalcogenide Letters **14**(9), 381 (2017).